Bioengineering cobalt chromium cardiovascular stent biomaterial for surface enhancement and characterization

Thamarasee Jeewandara [1]

[1]Sydney Medical School, University of Sydney

April 17, 2023

Abstract

Cobalt Chromium alloy L605 is an underlying biomaterial for most new generation drug eluting stents (DES) and bare metal stents (BMS). Suboptimal biocompatibility of stents clinically manifest as thrombosis and restenosis. We optimized a plasma-activated coating (PAC) technology to modify alloy L605 material surface (PAC-L605), for the first time, for enhanced biocompatibility. This study details in vitro characterization to identify and optimize the physical, chemical, and mechanical properties of the modified material surface PAC-L605. Surface hydrophilicity characterized post-modification with water contact angle and plasma kinetics, showed improved hydrophilicity for PAC-L605. Surface chemistry of PAC-L605 vs. L605, quantified with energy dispersive x-ray spectroscopy (EDS), showed comparatively higher weight percent of carbon and nitrogen on PAC surfaces. The microscale, isotropic surface roughness of PAC-L605, was computed with NanoMap white light interferometry (WLI). Surface stiffness computed via nanoindentation at minimum compression load 0.19 mN - increasing to maximum load 50 mN, showed similar stiffness for PAC-L605 and L605 at higher load. Nanoindentation results confirmed robust adhesion of PAC to L605, and unique non-delaminating character of PAC under compression. Furthermore, surface modification at PAC-L605 interface was visualized via high-resolution transmission electron microscopy (HRTEM). Improvements of surface character for implantable cardiovascular materials could be achieved by plasma-activated coating (PAC). Optimal surface modifications may trigger desirable biological responses in vitro and in vivo.

the WINNOWER

ENGINEERING

Bioengineering cobalt chromium cardiovascular stent biomaterial for surface enhancement and characterization

THAMARASEE JEEWANDARA [1]

1. *Sydney Medical School, University of Sydney*

Cobalt Chromium alloy L605 is an underlying biomaterial for most new generation drug eluting stents (DES) and bare metal stents (BMS). Suboptimal biocompatibility of stents clinically manifest as thrombosis and restenosis. We optimized a plasma-activated coating (PAC) technology to modify alloy L605 material surface (PAC-L605), for the first time, for enhanced biocompatibility. This study details *in vitro* characterization to identify and optimize the physical, chemical, and mechanical properties of the modified material surface PAC-L605. Surface hydrophilicity characterized post-modification with water contact angle and plasma kinetics, showed improved hydrophilicity for PAC-L605. Surface chemistry of PAC-L605 vs. L605, quantified with energy dispersive x-ray spectroscopy (EDS), showed comparatively higher weight percent of carbon and nitrogen on PAC surfaces. The microscale, isotropic surface roughness of PAC-L605, was computed with NanoMap white light interferometry (WLI). Surface stiffness computed via nanoindentation at minimum compression load 0.19 mN - increasing to maximum load 50 mN, showed similar stiffness for PAC-L605 and L605 at higher load. Nanoindentation results confirmed robust adhesion of PAC to L605, and unique non-delaminating character of PAC under compression. Furthermore, surface modification at PAC-L605 interface was visualized via high-resolution transmission electron microscopy (HRTEM). Improvements of surface character for implantable cardiovascular materials could be achieved by plasma-activated coating (PAC). Optimal surface modifications may trigger desirable biological responses *in vitro* and *in vivo*.

CORRESPONDENCE:
thamarasee@hotmail.com

DATE RECEIVED:
February 22, 2016

DOI:
10.15200/winn.145619.92147

ARCHIVED:
February 22, 2016

KEYWORDS:
Surface Engineering, Characterization, Plasma-activated coating, Biocompatibility, cardiovascular stents

CITATION:
Thamarasee Jeewandara , Bioengineering cobalt

INTRODUCTION

A principal requirement for biomedical alloys in device implantation is *in vivo* corrosion resistance, and optimal compatibility at the implant interface. In the context of materials science, biocompatibility is the ability of a material to assist a specific biological application and elicit an appropriate response, simulated *in vitro* or translated *in vivo*. The *in vivo* response of a device is dependent on the biological conditions it encounters (Bertrand et al. 1998). The objective of tissue engineering studies aim to assess biocompatibility of devices within physiological conditions *in vitro*, prior to their implantation in a preclinical, translational model *in vivo* (Waterhouse et al. 2012). Cobalt chromium super alloys are at present increasingly selected in the medical device industry as laser-cut, cardiovascular stents for implantation, as they meet three key selection criteria; 1. Reduced strut thickness for improved deliverability/device position *in vivo*, 2. Reduced total stent volume contributing to reduced restenosis 3. *In vivo* corrosion resistance and general biocompatibility (Cohen 1998).

While dual antiplatelet therapy (DAPT) and patient related arterial lesions (Cutlip et al. 2015), heavily influence sustained stent device compliance *in vivo*, the behavior of device alone depends on its material composition. Device characteristics are linked to physical, chemical and mechanical properties of the biomaterial used for its fabrication (Cohen 1998). In this study, we used an ASTM F90 wrought

chromium cardiovascular stent biomaterial for surface enhancement and characterization, *The Winnower* 3:e145619.92147 , 2016 , DOI: 10.15200/winn.145619.92147

alloy Co-20Cr-10Ni material with chemical composition listed in table 1. The alloy meets UNS R30605 specifications for medical applications, similar to biomaterial used to fabricate commercially available cardiovascular stents.

Clinical complications of late stent thrombosis (LST) undermine benefits of drug eluting stents (DES), proposing discriminate use of DES, alongside a recommended regime of DAPT (Lagerqvist et al. 2007, Slottow and Waksman 2007). Cobalt chromium stents (CCS) have shown clinically sound characteristics similar to DES; although they are comparatively more cost effective, have lowered rates of restenosis and LST (Youssef et al. 2010). Regardless of stent type implanted, a rigorous regime of prolonged (6 months or more) DAPT is required, to maintain device compliance and compatibility *in vivo* (Cutlip et al. 2015).

At present, materials science and tissue engineering research aim to create biocompatible implant surfaces for improved biointegration. The technical process utilized in this study, is a proprietary applied plasma physics technology that aims to render a material surface biocompatible, via energetic ion-assisted plasma deposition (Bilek and McKenzie 2010). The technique can 'biofunctionalize' a material surface for optimized biological outcome, demonstrated with applications of modified alloy 316L stainless steel (316LSS, ASTM F138) (Waterhouse et al. 2012, Bilek et al. 2011). Figure 1 schematically represents the applied plasma physics process of plasma-activated coating (PAC) deposition for material surface modification. The PAC surface modification is unique due its non-delaminating character (Waterhouse et al. 2010). In this study, we investigated the material characteristics of a plasma modified cobalt chromium alloy L605 (PAC-L605), in comparison to its bare metal form (L605), for the first time. We analyzed the physical, chemical and mechanical character of the commercially available, plasma-modified medical biomaterial, using techniques of applied plasma physics and materials science.

MATERIALS AND METHODS

PREPARATION OF COBALT CHROMIUM ALLOY L605 FOR SURFACE MODIFICATION

Samples of alloy L605 (10 cm x 8 cm x 0.025 cm) were washed in three reagents: 70% v/v ethanol, absolute acetone and phosphate buffered saline (PBS), 15 minutes each prior to plasma activated coating (hitherto referred to as PAC) deposition. All experiments were carried out with freshly made PAC, used within 2 weeks, unless stated otherwise.

Table 1: Chemical composition of commercially available cobalt chromium alloy L605 for surgical implant applications [as represented in (Poncin P 2004)]

Element	Percent Weight (Wt%)
Carbon (C)	0.112
Chromium (Cr)	20.10
Cobalt (Co)	BAL
Iron (Fe)	2.40
Manganese (Mn)	1.51
Nickel (Ni)	10.70
Tungsten (W)	14.70
Phosphate (P)	0.010
Sulphur (S)	<0.002
Silicon (Si)	0.20
Specifications: AMS 5537, H; ASTM F90-09 Chemistry only, UNS# R30605	

SYNTHESIS OF PLASMA-ACTIVATED COATING

Fused silica (10 cm x 8 cm x 0.05 cm) was coated with the same PAC recipe, alongside samples of alloy L605, as a reference material. The cleaned substrates were mounted onto a stainless steel cylindrical ccrf reactor. Base pressure of the system was pumped down to 10^{-6}-10^{-5} Torr. A reactive mixture of argon, nitrogen and acetylene plasma was introduced in the upper part of the reactor. The flow, Q, of each gas for alloy L605 surface; QArgon=3 sccm, QAcetylene=1 sccm, and QNitrogen=10 sccm (500 V, t=20 min), was controlled individually, using mass flow controllers and maintained constant, during coating deposition (PAC1 recipe). On another alloy L605 sample of similar dimensions, we trialed a second recipe QArgon = 3 sccm, QAcetylene = 2 sccm and QNitrogen = 10 sccm (1000 V, t = 10 mins) (PAC2 recipe). Plasma was sustained at a total pressure of 80 mTorr, rf power 50 W, and deposition time of 10-20 mins. Unless specified, both PAC 1 and PAC 2 recipe surfaces were characterized alternatively in the preceding studies.

SURFACE PROFILOMETRY

Thickness of PAC recipes deposited on L605 and reference Si wafer surface was measured on the reference material, with surface profiler Dektak 3030 (Bruker, Germany).

PLASMA KINETICS TO ASSESS SURFACE HYDROPHILICITY

The sessile drop technique was used for contact angle measurements of a modified surface with DS10 Kruss contact angle goniometer (Kruss GmbH, Germany). After 15 min of PAC deposition, the modified material was placed on the goniometer platform, and a water drop introduced to the surface via a microsyringe. The three-phase contact line of the drop, made with drop shape analysis (DSA) software was measured with a microscope, at room temperature. Measurements were repeated for three liquids, water, diiodomethane and formaldehyde respectively. All measurements were conducted 15 min post deposition up to 40,320 min (4 weeks) of storage. Average contact angle of five measurements, at each time point, of any two liquids (water and diiodomethane), were used to compute correlating surface energy and its components (polar and dispersive parts) with the regression method/Owens-Wendt-Rabel-Ström kinetic model (DSA software). Results were compared with previously recorded measurements of a similar PAC recipe on alloy 316L SS, within a 15 min – 20,160 min (2-week) period.

ELECTRON DISPERSIVE X-RAY SPECTROSCOPY TO ASSESS SURFACE CHEMISTRY

Samples of PAC-L605 (recipes 1 and 2) were comparatively imaged alongside bare metal alloy L605 (0.8 cm x 0.8 cm, sample size), using a Zeiss-Ultra field emission scanning electron microscope (Zeiss, Germany). Surface chemistry at the nanoscale was analyzed with Aztec software (Oxford Instruments, UK), at an acceleration voltage of 2 kV, 11 mm working distance, and 2000 X-ray cps. Weight percent of the elements predominant to the three different sample surfaces were quantified independently for an average of three sites, on each surface.

NANOMAP WHITE LIGHT INTERFEROMETER (WLI) TO ASSESS SURFACE ROUGHNESS

Surface roughness measurements of the modified material was quantified using NanoMap-1000 WLI, 3D optical profilometry (AEP technology, Santa Clara, CA, USA). The PAC-L605 sample (0.6 cm x 0.6 cm) was mounted on a computer controlled sample stage, located on a vibration-isolated table (air pressure 1 atm). The sample was magnified with 10 x objective optical microscope, atop the sample stage. Field of view was chosen using the computer controlled motorized NanoMap optical software, for a 100 µm Z range and 1 mm x 1 mm scanning area of sample at 1 x scan speed. Initial optical image obtained was re-opened in image software PIPS 6.0.14, to generate 3 D image of topographical data, with zero background and global levelling. Optical image was next opened with Gwyddion 2.41 software for scanning probe microscopy (SPM) data analysis (Dept. of Nanometrology, Czech Metrology Institute). Using the automated 'Statistical quantities' tool, roughness measurements (RMS) for sample surface at 5 different surfaces were calculated and averaged.

NANOINDENTATION TO ASSESS SURFACE STIFFNESS

Surface stiffness of modified material (PAC1-L605) was calculated and compared to the surface stiffness of bare cobalt chromium alloy L605 (2 cm x 1 cm x 0.05 cm). Force-controlled nanoindentation, was conducted using a Hysitron Triboindenter (G200, Agilent) fitted with a Berkovich diamond indenter (TB22122, m0 24.7772) with a radius of curvature R. Nanoindentation was conducted from a minimum load of 0.19 mN to a maximum load of 50 mN for 100 indents, at randomly chosen positions on each surface. Indentations were made under the same conditions to confirm uniformity of mechanical properties of entire surface coating. Surface stiffness was measured as a log function of the unload depth (D) (nm) vs. load, as a function of force (F) mN, equation 1 from (Oliver and Pharr 2004).

$S = \Delta F/\Delta D$

The unloading displacement for 21 indentations were batch processed using a Matlab Mathworks version 8.5 (MA, USA). The algorithm to calculate surface stiffness was developed by Dr. Yixiang Gan's research group, Civil Engineering, University of Sydney (Appendix A).

FOCUSED ION BEAM (FIB) MILLING TO PREPARE AN ELECTRON-TRANSPARENT PAC-L605 LAMELLAE

The modified sample material of interest (sample dimensions: 1 cm x 1 cm x 0.025 cm) was mounted on a half-grid and inserted vertically to the FIB chamber (Zeiss, Auriga). Before milling, a platinum (Pt) line was deposited over the surface area of interest marking position of target area. An initial incidence angle of ± 4^{o} was used in perpendicular exposure of sample at 30 kV milling voltage and 25 pA current, to mill down modified metal sample to a thickness of ~150 nm. The incidence angle was increased to ± 6^{o} at a voltage of 5 kV and current of 10 pA, until further thickness of 80 nm was achieved. Residual milling to obtain a cross-section of 20 nm thickness was conducted at ± 8^{o}, 5 kV for remaining material. The final electron transparent lamellae seen from above appears as a cross bar in the form of letter 'H', referred to as H-bar technique during lift out, and transferred for high resolution transmission electron microscope (HRTEM) imaging. The electron transparent, 20 nm PAC-L605 sample lamellae cross-section, prepared within FIB, was lifted out and attached to a copper half-grid to transfer to the sample holder of the HRTEM.

HIGH RESOLUTION TRANSMISSION ELECTRON MICROSCOPY (HRTEM) TO ANALYZE PLASMA COATING-BIOMATERIAL INTERFACE.

The FIB milled electron transparent sample was placed on the JEOL double hilt high background TEM sample holder 'JEM-2200 FS HRTEM' (JEOL, San Francisco, CA, USA). The 20 nm thick cross-section of plasma modified PAC-L605 lamellae was imaged at a 200 kV field emission gun acceleration voltage, 95.5 µA (dark current), and 52.0 µA (Emission current) up to 1.1 Å atomic resolution and 1.2 M magnification. Alloy L605 bare metal underlying PAC deposition was imaged separately to visualize alloy microstructure, with selected area electron diffraction (SAED). An Inverse Fast Fourier Transform (IFFT) pseudo color image of the PAC-L605 cross-section was obtained to visualize detailed microstructure at interface. Electron energy loss spectroscopy (EELS) was conducted with zero-loss peak (ZLP) omega filter, for reliable measurement of local thickness, and verification of chemical composition at interface. The thickness was calculated as mfp*ln(I/I0), where mfp is the mean free path of electron inelastic scattering, tabulated for most elemental solids and oxides (Gatan Inc, Japan)(Iakoubovskii et al. 2008) and I/I0 are integrals under the whole spectrum and under the ZLP, respectively.

STATISTICS

Data are expressed as mean± standard error of the mean. Data were analyzed by paired t-test for statistical significance, using GraphPad Prism version 6.00 (GraphPad software, San Diego, CA, USA) for MAC OS X.

RESULTS AND DISCUSSION

SURFACE COATING THICKNESS

The PAC1-L605 surface coating profilometry trace thickness was measured as 20 nm. The PAC2-L605 surface coating profilometry trace thickness was measured as 10 nm. The time of PAC deposition (20 min and 10 min respectively), correlated to the thickness of surface coating characterized. The rate of PAC deposition was 1 nm/min.

SURFACE PLASMA KINETICS

The initial water contact angle, 15 min post PAC-L605 modification was 44.4°±3.41, by 2 weeks the contact angle increased to 89.98°±3.78, and by 4 weeks to 92.96°±1.38. Results summarized in table 2 and represented in figure 2 A. Correlating surface energy calculated 15 min post PAC deposition was 62.35±2.43 mJ/m^2, by 2 weeks 32.22±2.88 mJ/m^2, and by 4 weeks 28.96±1.20 mJ/m^2. Results were compared with previous plasma kinetics study of a similar PAC recipe deposited on alloy 316L SS within a study period of 15 min-20,160 min (2 weeks) (Figure 2 B). Water contact angle for PAC-316LSS was 57.86°±0.48, by two weeks the contact angle increased to 84.66° ±0.33. Correlating surface energy calculated 15 min post PAC-316LSS deposition was 52.02±0.05mJ/m^2, and decreased to 37.68±0.01mJ/m^2 at two weeks. Figure 3 indicates variation of the components of surface energy (polar and dispersive), contributing to total surface energy. The polar energy decreased significantly over time from 22.62 mJ/m^2 to 3.15 mJ/m^2, although the dispersive part did not change much from 39.62 mJ/m^2 to 29.11 mJ/m^2.

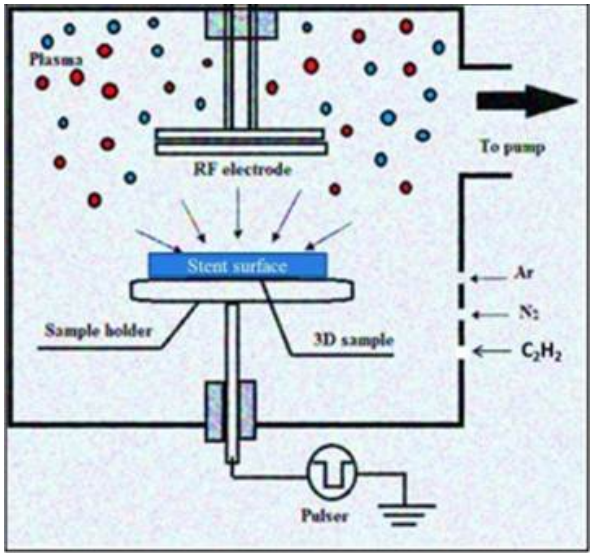

Figure 1: Plasma surface modification for coronary stents from (Jeewandara, Wise, and Ng 2014). Nitrogen, argon and acetylene plasma gases were introduced into a chamber under vacuum, and ionized by a power source such as RF electrode. Charged ions in the chamber impact substrate to modify surface immersed in plasma.

Table 2: Comparative water contact angle and surface energy measurements for PAC modified biomaterial alloy L605 within a period of 15 min – 40,320 min (4 weeks) and alloy 316L within a period of 15 min-20,160 min (2 weeks)

Biomaterial	Surface Hydrophilicity			Surface energy mJ/m²		
	15 min	20,160 min	40,320 min	15 min	20,160 min	40,320 min
PAC-L605	44.4°±3.41	89.98°±3.78	92.96°±1.38	62.35 ±2.43	32.22 ±2.88	28.96 ±1.20
PAC-316LSS	57.86°±0.48	84.66°±0.33	-	52.02 ±0.05	37.68 ±0.01	-

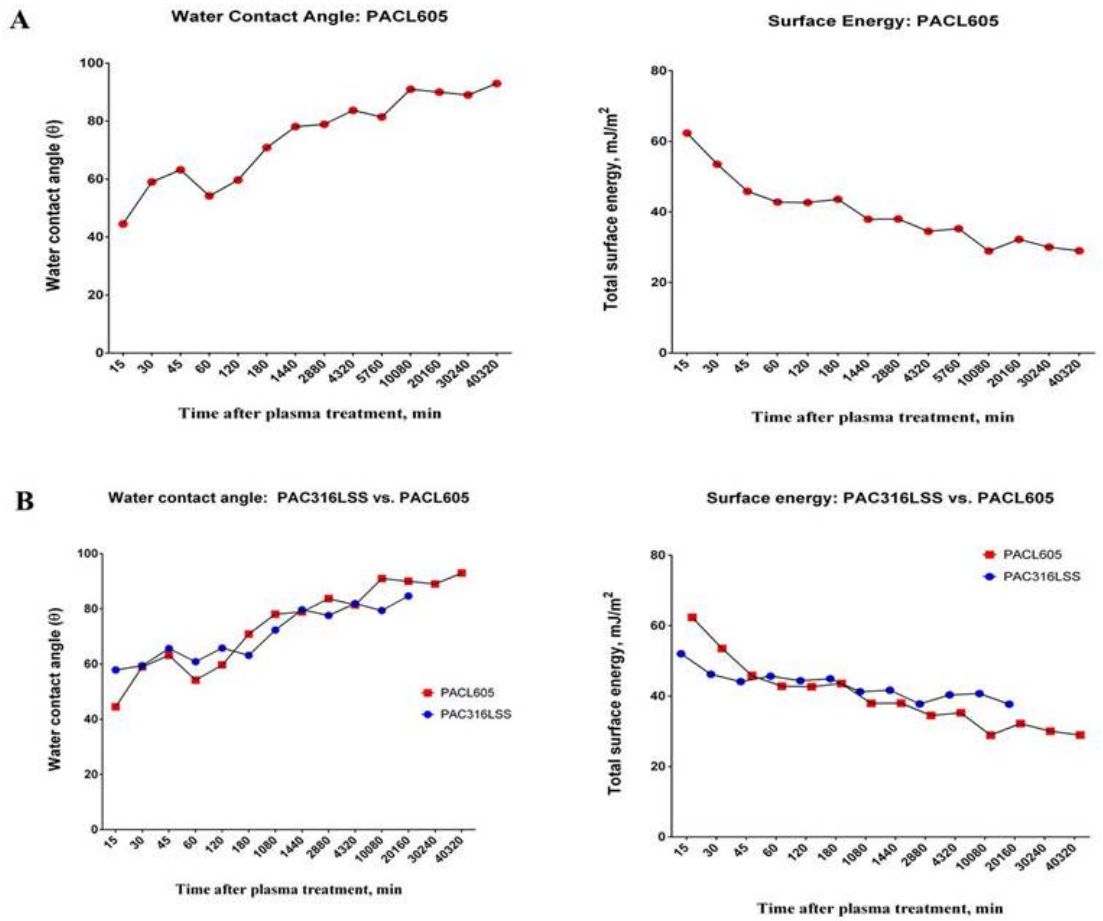

Figure 2: A) Water contact angle for PAC-L605, increased within a period of 15 min-40,320 min (4 weeks) to reach plateau, correlating surface energy decreased within the same period to reach plateau. B) The PAC-L605 results were compared with PAC-316LSS (previously recorded), within a time-frame of 15 min-20,160 min (2 weeks) for similar trends in water contact angle and surface energy variation, respectively.

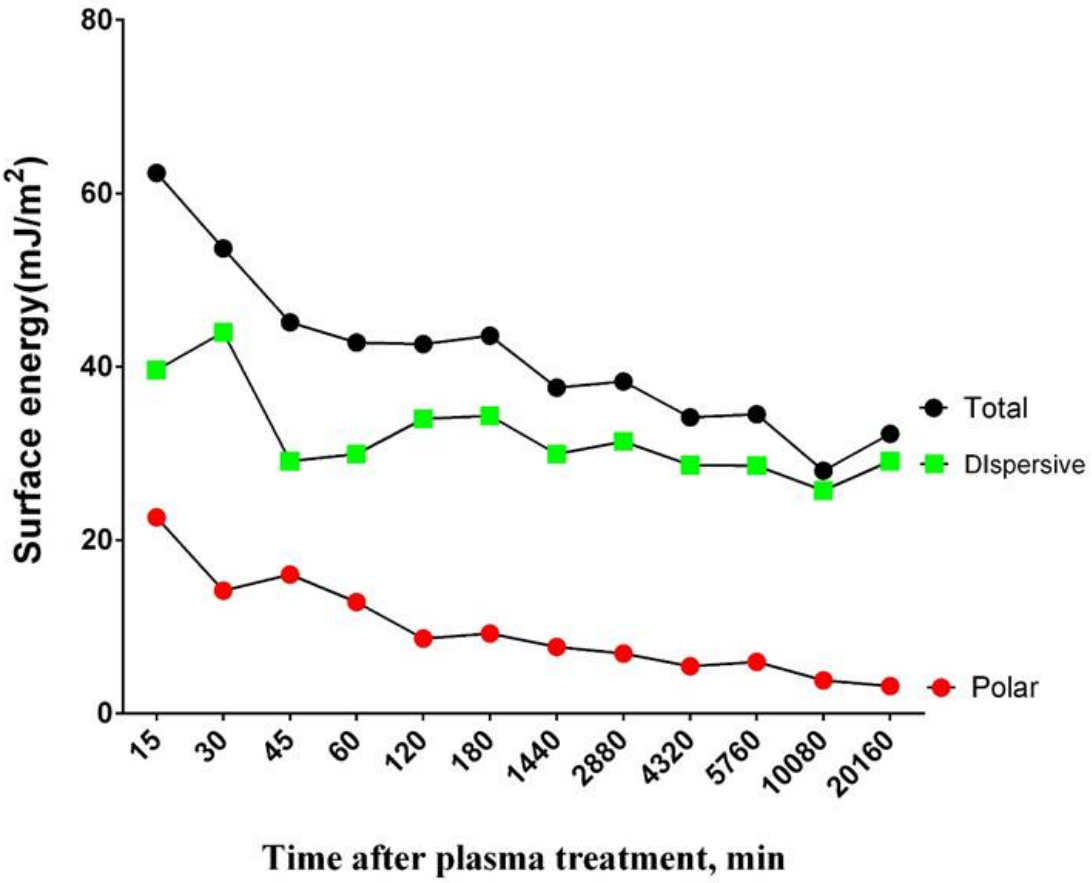

Figure 3: Variation of total surface energy and its contributing components (polar and dispersive), 2 weeks after plasma treatment (15 min-20,160 min) of PAC-L605. The polar surface energy component decreased dramatically with time, in contrast to the decrease observed with dispersive surface energy.

SURFACE CHEMICAL COMPOSITION

Initially chemical composition of stainless steel alloy 316L was compared to cobalt chromium alloy L605. Alloy 316L SS had a predominant Iron (Fe) weight percent (48.50%), in contrast to alloy L605 (1.77%). Alloy L605 had a high Cobalt (Co) weight percent (34.96%), and alloy 316LSS did not constitute cobalt in its composition (Figure 4 A). Surface chemistry of PAC recipe 1 (C-1, N-10, 500 V, t-20 min) was compared to PAC recipe 2 (C-2, N-10, 1000 V, t-10 min) and bare metal alloy L605. The PAC recipe 1 modified surface, had significant weight percent of nitrogen (N) (3.03%), and carbon (C) (9.20%), compared to surface chemistry of PAC recipe 2; nitrogen (0.60%), carbon (2.96%) ($p<0.05$). The unmodified bare metal alloy L605 included; nitrogen (0.00%) and carbon (1.60%) among other percentages of elements (Figure 4 B).

SURFACE ROUGHNESS – NANOMAP WHITE LIGHT INTERFEROMETRY (WLI) TECHNIQUE

Surface roughness was measured for 5-10 separate positions on PAC-L605 modified surface, at 100 µm x 100 µm areas with NanoMap WLI technique. The NanoMap 3D topography images constructed are in figure 5. The average roughness computed with WLI mechanical profiler Gwyddion software was 0.272 µm.

SURFACE STIFFNESS AND COATING INTEGRITY – NANOINDENTATION

Two samples of interest; PAC-L605 with a 20 nm coating (PAC 1 recipe), and alloy L605 bare metal, were analyzed to compare surface stiffness. Figure 6 shows surface stiffness at lowest indentation load of 0.19 mN (~ 2 mN) for PAC as 0.0036 mN/nm, and for bare metal alloy L605 as 0.051 mN/nm ($p<0.05$). With increasing indentation load (>3 mN) surface stiffness increased similarly, on both

surfaces. At maximum load of 50 mN, surface stiffness was similar for PAC as 0.013 (0.012492) mN/nm and for L605 as 0.013 (0.012652) mN/nm.

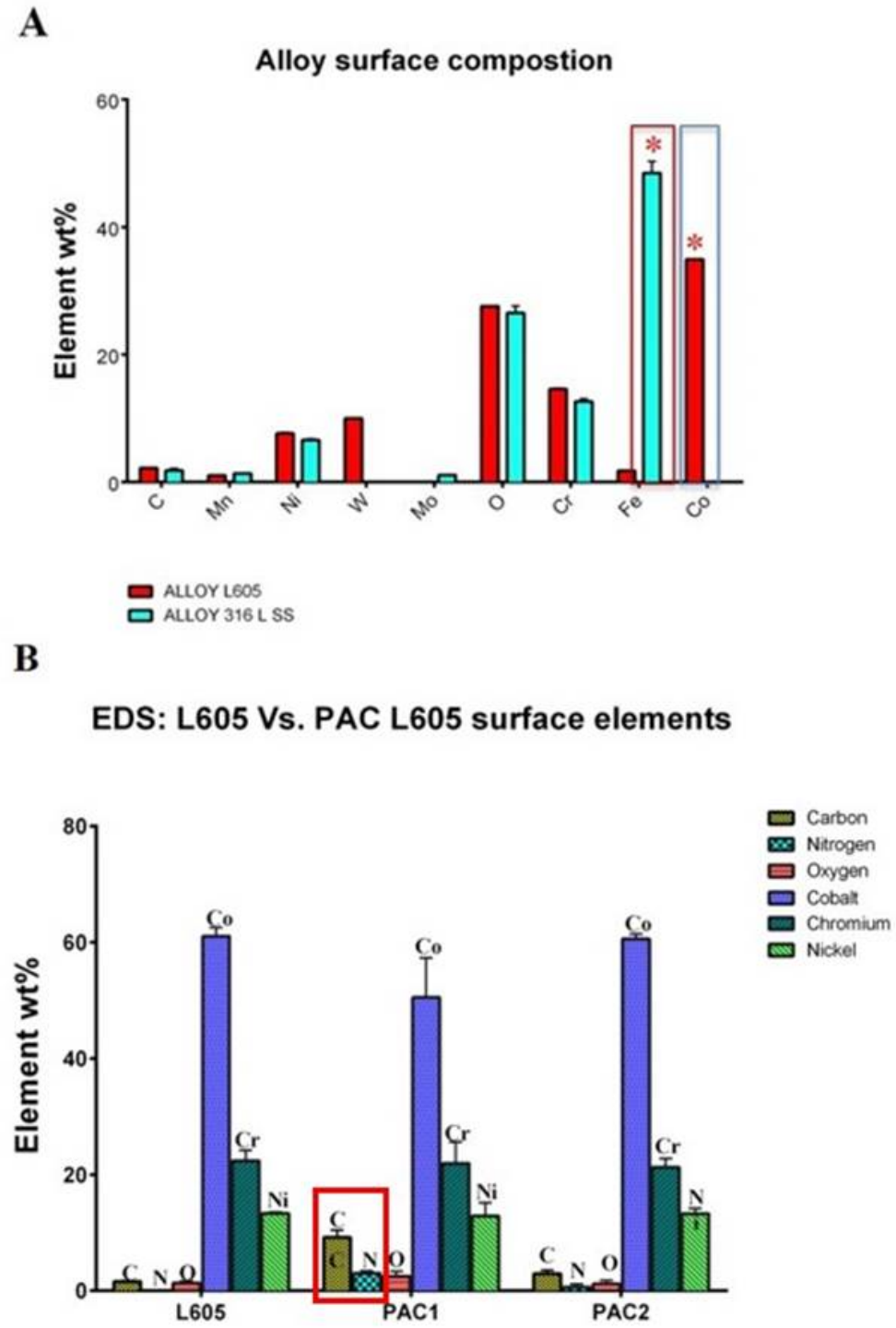

Figure 4: A) Surface chemical composition of cobalt chromium alloy L605 (ASTM F90) and stainless steel alloy 316LSS (ASTM F138) – show predominant Co and Fe peaks respectively. B) Plasma recipe 1 (C-1, N-10, t=20 min, 500 V) shows higher C and N content compared to plasma recipe 2 (C-2, N-10, t=10 min, 1000 V) and bare metal alloy L605.

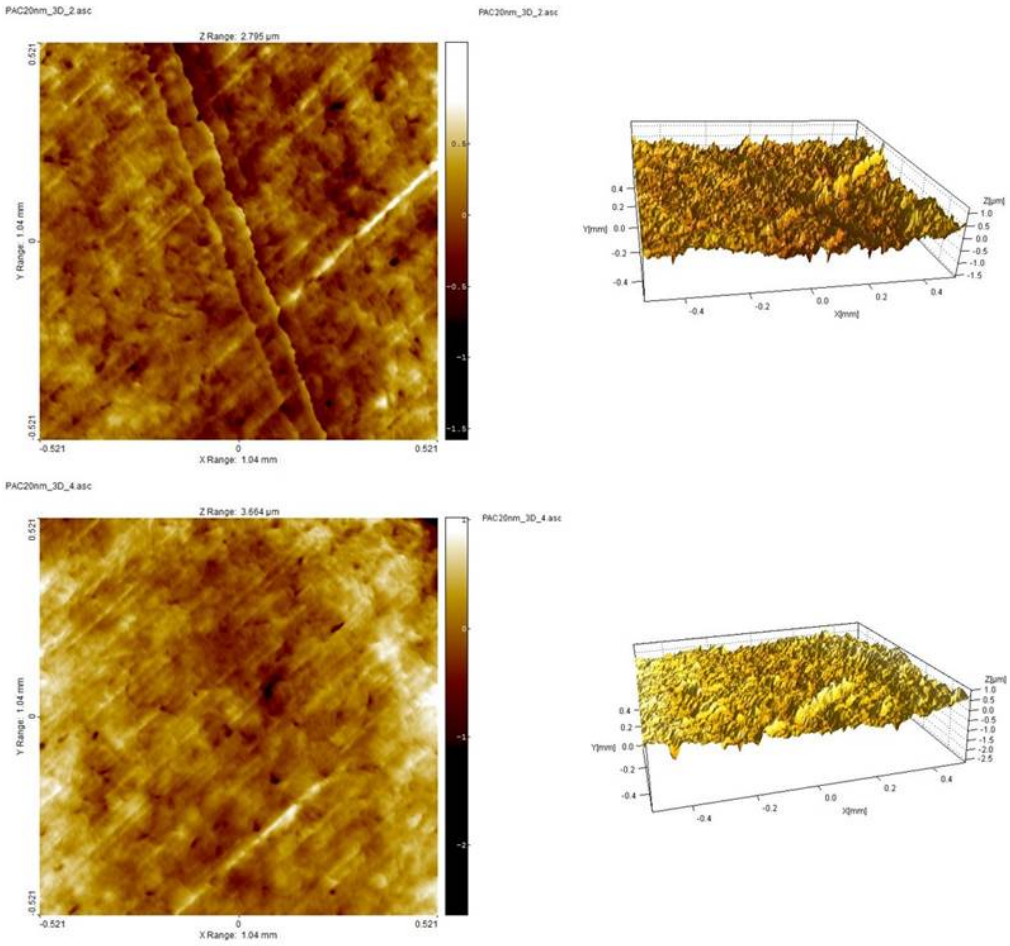

Figure 5: NanoMap WLI images of PAC-L605 surfaces imaged at 10 x objective, within a 100 µm x 100 µm (0.01 cm x 0.01 cm) scanning area. The images were converted to 3D topographical surface representations (Gwyddion software) and roughness measured with statistical tool (measurements not shown).

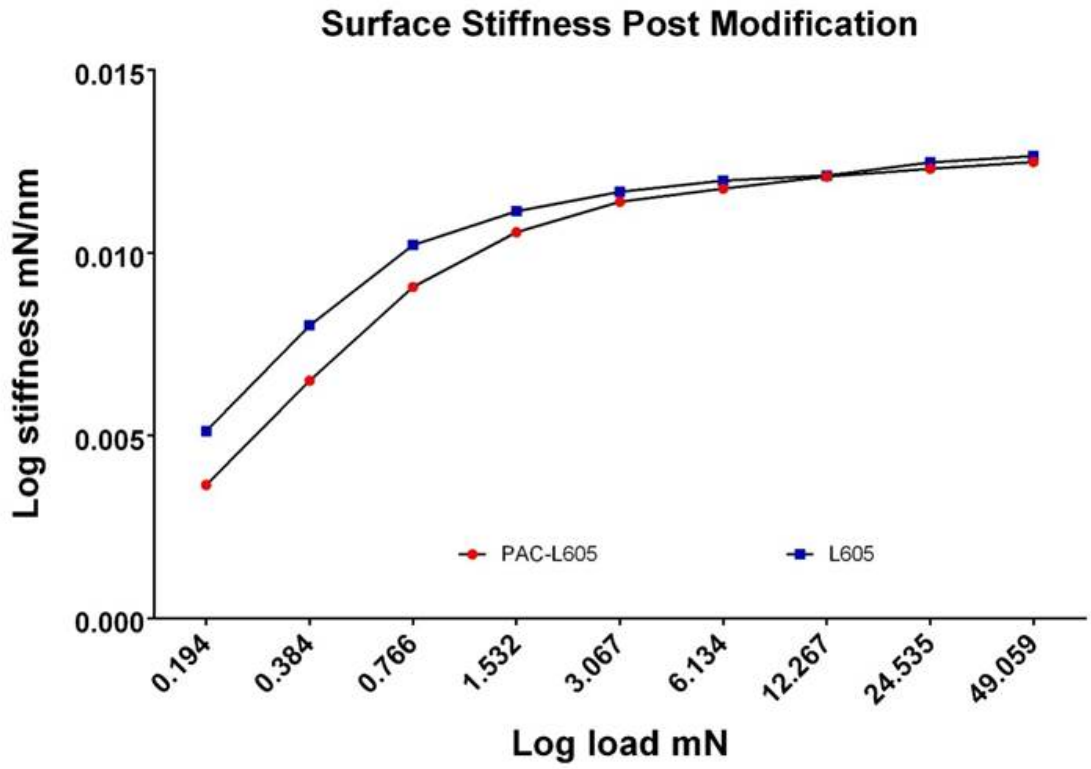

Figure 6: Nanoindentation measurements comparing PAC-L605 (20 nm coating) with bare metal alloy L605 surface stiffness, for an average of 20/100 indents each. Minimum load used 0.19 mN and maximum load 50 mN. At minimum load (0.19 mN), PAC-L605 stiffness is lower than bare metal alloy L605. With increasing load, stiffness of the coating remains similar to metal alloy, displaying surface coating integrity to underlying material, and coating non-delamination at highest load 50 mN.

SURFACE COATING INTEGRITY – HIGH RESOLUTION TRANSMISSION ELECTRON MICROSCOPY (HRTEM)

Focused Ion Beam (FIB) milling of a sample of plasma-modified material (PAC-L605) with 20 nm thick electron transparent lamellae, was prepared for interface imaging with HRTEM (Figure 7). Figure 8 A, shows HRTEM image at cross-sectional interface, with plasma polymer deposited on crystalline cobalt chromium material. The white (electron transparent) layer is PAC, capped with a thin platinum layer deposited during FIB milling (not shown in image). In Figure 8 B, an Inverse Fast Fourier Transform (IFFT) image of PAC-L605 interface (with pseudo color), shows a distinct buffer layer/ion stitching boundary at the PAC-L605 interface (green), as theorized during PAC deposition and free radical surface functionalization (Bilek et al. 2011). In the IFFT image, the plasma coating (yellow) adheres to alloy L605 (blue) via ionic stitching/buffer layer (green) at the plasma-metal interface. The bare crystalline cobalt chromium metal was selectively imaged independent of PAC, via electron diffraction to show twinning at the grain boundaries, characteristic to alloy L605 material (Figure 9). The characteristic feature of alloy L605 had been previously described via SEM imaging (Poncin P 2004). The electron energy loss spectra (EELS) showed an overall thickness of 47.84 nm for Platinum (Pt), 35 nm for Carbon (C), and 66.67 nm for Cobalt (Co), confirming interface thickness/composition (Bilek et al. 2011) (Figure 10). For simplicity, regions of the material interface in the HRTEM image were color segregated, to represent elemental composition and thickness as identified via EELS (Figure 10).

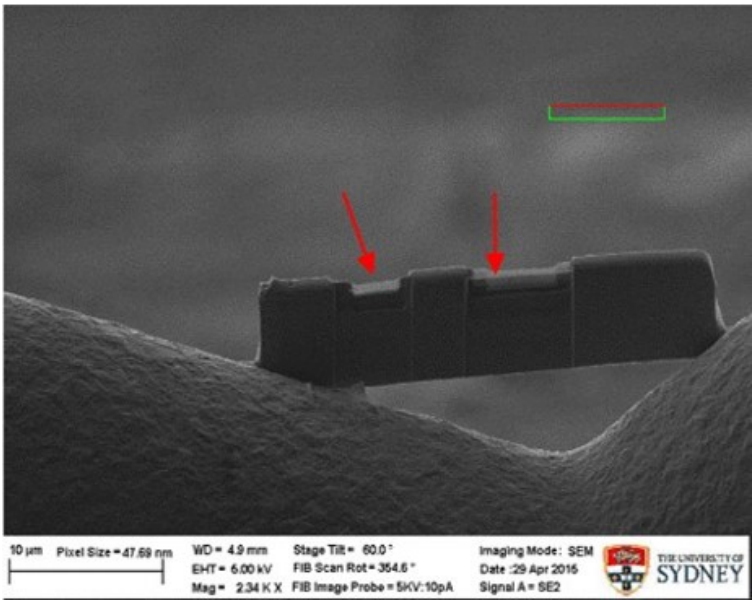

Figure 7: The FIB milled, plasma modified, PAC-L605 sample, with two regions of electron transparent lamellae at the modified material interface, milled to 20 nm thickness (red arrows, 2.3 K x mag, 5 kV) in preparation for HRTEM imaging.

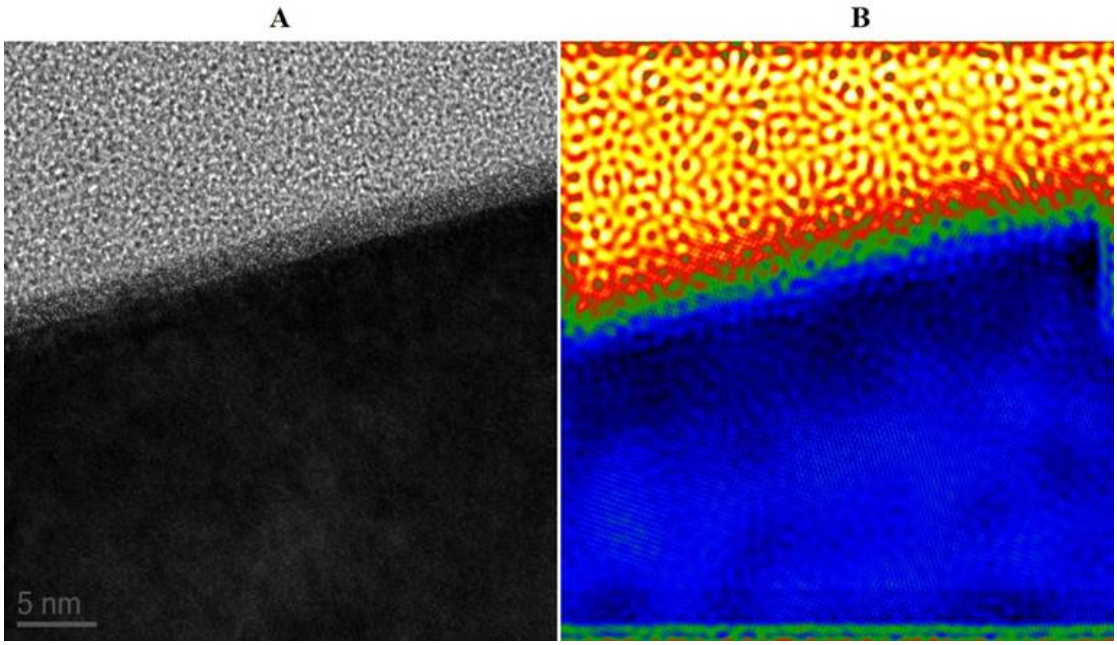

Figure 8: A) Cross section of PAC-L605 interface: The HRTEM image with white (electron transparent) polymer deposit, crystal metal alloy (black) and ionic stitching at interface (grey). B) Corresponding IFFT image shows plasma coating (yellow) adheres to alloy L605 (blue) via ionic stitching buffer layer (green) at the plasma-metal boundary (interface). Magnification 1.2 Mx, 1.1 Å resolution, 200 kV).

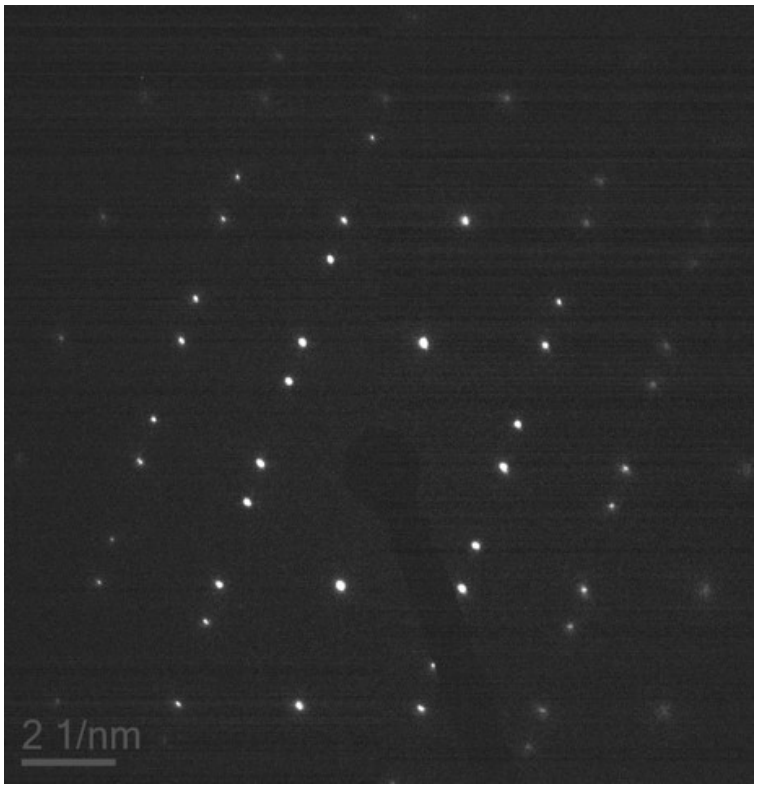

Figure 9: Selected area electron diffraction (SAED) of the alloy L605 cobalt chromium metal matrix. The region imaged is below the 20 nm cross-section of PAC-L605 interface. Material matrix shows presence of crystal twinning within metal alloy microstructure.

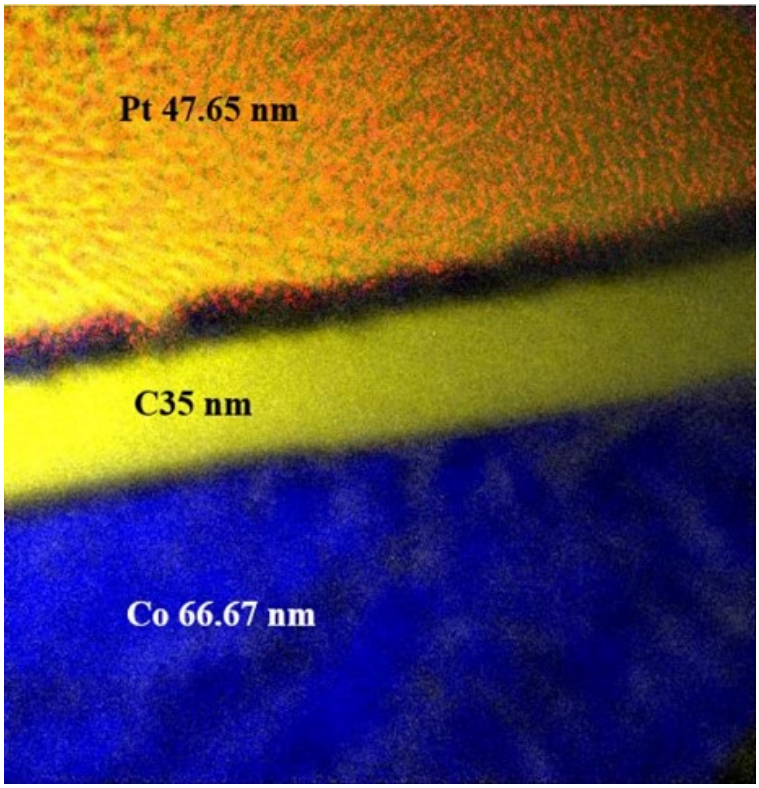

Figure 10: Chemical composition of the PAC-L605 interface represented via color segregation on HRTEM image (2.3 K x mag). Thickness of elements represented at the interface were calculated with electron energy loss spectra EELS. Thickness of elements observed in the interface were platinum (Pt) 47.65 nm (deposited during FIB milling to protect modified PAC surface), carbon (C) 35 nm, and cobalt (66.67 nm).

CHARACTERIZING PAC PROPERTIES ON ALLOY L605

Overall, this study characterized the sample interface of alloy L605 deposited with PAC (PAC-L605), via physical, chemical and mechanical methods post-modification. Quantitative surface chemistry characterization with EDS utilized a very low accelerating voltage of 2 kV. The low voltage ensured electrons from the primary beam only penetrated the surface of modified material (20 nm or 10 nm thickness), to interact with surface atoms alone, and not underlying biomaterial. The quantified elemental X-ray intensities, verified the chemical composition of plasma-activated surface modifications, compared to its bare metal form.

The inconsistent, isotropic, microscale surface roughness, observed and quantified with NanoMap WLI is due to the proprietary plasma polymerization process of deposition and consecutive etching (Yin et al. 2009). The technique of optical profilometry for surface roughness measurement of engineered surfaces is based on physical principles of the wave properties of light (Ali 2012).

Surface roughness of a modified material has a strong influence on its surface wetting character (hydrophilicity). The untreated alloy L605 is strongly hydrophobic with an estimated water drop wetting angle approximating $>100^0$ (Mills report for alloy L605). Immediately after plasma treatment (15 min), the water contact angle for PAC-L605 decreased, alongside increased correlating surface energy. Similar trends were observed within a 2-week period for both biomaterials modified with PAC (PAC-L605 and PAC-316LSS). Decreasing polar and dispersive energy components contributed to decreasing total surface energy, with time. With exposure to air, dispersive surface energy, representing surface oxidation decreased lesser with time, compared to polar surface energy representing surface free radicals, which varied greatly. This variation was expected since surface free radicals undergo oxidation, with exposure to air over time (Bilek et al. 2011). The timeline of the plasma kinetics study was similar to previous studies (Bilek et al. 2011, Kondyurin et al. 2012), although characterized for the first time with modified cobalt chromium - PAC-L605. Mildly hydrophilic material surface modifications are at an advantage *in vivo*, as they display favorable interactions with proteins, cells, blood, and decrease platelet adhesion (Seeger et al. 1995, Waterhouse et al. 2012). Stent surface polymer incompatibility can trigger a vascular response of inflammation, and neointima formation - as seen with DES (Carter et al. 2004). Polymer hydrophilicity and surface biocompatibility are essential for successful stent biointegration.

UNIQUE FEATURES OF PLASMA TECHNOLOGY SUITED TO MODIFY COBALT CHROMIUM STENTS

At present bare metal alloy L605 is used to fabricate commercially available cobalt chromium stents ML8 (Vascular 2012). Among other benefits, higher content of cobalt in alloy L605 contributes to increased radiopacity and assists coronary stent implantation *in vivo*. During the process of stent implantation and revascularization *in vivo*, stents undergo large strains and must remain as a permanent scaffold with an intact surface polymer or coating. Clinically, new generation DES have failed to withstand challenges of large strains, resulting in damage to the abluminal polymer, requiring stent replacement (Fujimoto, Kobayashi, and Yamaguchi 2012). Polymer layer defects are a persistent concern with commercially available stents as observed via SEM analysis (Otsuka et al. 2007, Ormiston 2005). Clinical complications of polymer delamination *in vivo* lead to increased risk of thrombosis, interruptions to drug pharmacokinetics dose released via polymer, trigger an inflammatory response, and cause micro-embolism (Hopkins, McHugh, and McGarry 2010, Kollum et al. 2005).

Parameters governing stent coating delamination include; coating thickness, stiffness and integrity of surface coating or polymer at stent-material interface (Hopkins, McHugh, and McGarry 2010). The traditional method of nanoindentation was used to quantify mechanical properties of materials with thin

film coatings (Abdul-Baqi and Van der Giessen 2002, 2001). The system we investigated here was similarly composed of two materials with different mechanical properties. Failure to integrate different systems physically result in plastic deformation, cracking of the coating, or failure at the interface (Abdul-Baqi and Van der Giessen 2002). At minimum load, PAC-L605 exhibited lower stiffness compared to bare metal alloy L605, because of its 20 nm, soft surface plasma coating. With increasing load (3 mN-50 mN), the coating did not delaminate or crack, and both surfaces exhibited similar stiffness to quantitatively confirm plasma coating integrity to underlying material.

The HRTEM and corresponding IFFT images of PAC-L605 interface showed a distinct ionic buffer layer at the interface, detailing ionic stitching attachment of PAC to the metal, as theorized in applied plasma physics (Bilek and McKenzie 2010, Bilek et al. 2011). Surface composition of plasma coating on alloy L605 interface visualized with TEM supports surface integrity quantified earlier with nanoindentation. The individual layer thickness of elements at the PAC-L605 interface were re-confirmed with EELS.

Characteristic twinning between grain boundaries of cobalt chromium crystals observed with SAED, were in similarity to SEM images of grain boundary microstructure for alloy L605 (Poncin P 2004). The metal alloy remains unchanged post-surface modification with PAC. The modified novel material PAC-L605 is suitable for intended biological applications. We predominantly used PAC1 recipe surfaces for characterization due to increased C, N content and higher coating thickness. Further studies will include comparative investigations of PAC recipes 1 and 2, alongside bare metal alloy L605, for biological studies *in vitro*, followed by translational studies with an optimized recipe of PAC-cobalt chromium stent surface *in vivo* (Waterhouse et al. 2012).

CONCLUSION

The characterization of a plasma-modified material (PAC) confirmed surface hydrophilicity and coating integrity on cobalt chromium alloy L605 (PAC-L605), for the first time in this study. The unique non-delaminating nature of PAC on cobalt chromium was investigated via nanoindentation and HRTEM. The surface modification was non-brittle, soft and strongly adhered to underlying bare metal alloy L605 via ionic stitching at interface, preventing delamination under stress. The surface engineering technique enabled quantifiable changes in surface chemistry, surface kinetics and mechanics for improved biocompatibility of PAC-L605 compared to its bare metal alloy L605. Improvements of surface character for implantable cardiovascular materials could be achieved by plasma-activated coating (PAC).

ACKNOWLEDGEMENTS:

The manuscript was originally produced as part of thesis for Doctor of Philosophy (PhD) in Medicine, Sydney Medical School, University of Sydney - September 2015. Initial research work, was presented at the Atherosclerosis, Thrombosis and Vascular Biology (ATVB) Scientific conference, American Heart Association, San Francisco, CA, USA, May 2015 (DOI: 10.7490/f1000research.1111024.1). The author acknowledges

Applied Plasma Physics Department of the University of Sydney, for plasma-activated coating (PAC) development.

Research group of Dr. Yixiang Gan for research support in Civil Engineering, University of Sydney.

The Australian Center for Microscopy and Microanalysis (ACMM), University of Sydney, for research and technical support; Mr. Steven Moody (SEM specialist), Dr. Hongwei Liu (HRTEM specialist) and Dr. Patrick Trimby (SEM specialist).

Study funded by the National Health and Medical Research Council (APP1033079 and APP1039072), and PhD tenure: Elizabeth and Henry Hamilton-Browne Scholarship, Faculty of Medicine, Sydney Medical School.

REFERENCES

Abdul-Baqi, A., and E. Van der Giessen. 2001. "Indentation-induced interface delamination of a strong film on a ductile substrate." *Thin Solid Films* 381 (1):143-154. doi: Doi 10.1016/S0040-6090(00)01344-4.

Abdul-Baqi, A., and E. Van der Giessen. 2002. "Numerical analysis of indentation-induced cracking of brittle coatings on ductile substrates." *International Journal of Solids and Structures* 39 (6):1427-1442. doi: Pii S0020-7683(01)00280-3

Doi 10.1016/S0020-7683(01)00280-3.

Ali, Salah H. R. 2012. "Advanced Nanomeasuring Techniques for Surface Characterization." *ISRN Optics* 2012:23. doi: 10.5402/2012/859353.

Bertrand, Olivier F., Rajender Sipehia, Rosaire Mongrain, Josep Rodés, Jean-Claude Tardif, Luc Bilodeau, Gilles Côté, and Martial G. Bourassa. 1998. "Biocompatibility aspects of new stent technology." *Journal of the American College of Cardiology* 32 (3):562-571. doi: 10.1016/S0735-1097(98)00289-7.

Bilek, M. M. M., D. V. Bax, A. Kondyurin, Y. B. Yin, N. J. Nosworthy, K. Fisher, A. Waterhouse, A. S. Weiss, C. G. dos Remedios, and D. R. McKenzie. 2011. "Free radical functionalization of surfaces to prevent adverse responses to biomedical devices." *Proceedings of the National Academy of Sciences of the United States of America* 108 (35):14405-14410. doi: 10.1073/pnas.1103277108.

Bilek, Marcela M., and David R. McKenzie. 2010. "Plasma modified surfaces for covalent immobilization of functional biomolecules in the absence of chemical linkers: towards better biosensors and a new generation of medical implants." *Biophysical Reviews* 2 (2):55-65. doi: 10.1007/s12551-010-0028-1.

Carter, A. J., M. Aggarwal, G. A. Kopia, F. Tio, P. S. Tsao, R. Kolata, A. C. Yeung, G. Llanos, L. Dooley, and R. Falotico. 2004. "Long-term effects of polymer-based, slow-release, sirolimus-eluting stents in a porcine coronary model." *Cardiovascular Research* 63 (4):617-624. doi: 10.1016/j.cardiores.2004.04.029.

Cohen, J. 1998. "Current concepts review. Corrosion of metal orthopaedic implants." *J Bone Joint Surg Am* 80 (10):1554.

Cutlip, D. E., D. J. Kereiakes, L. Mauri, R. Stoler, and H. L. Dauerman. 2015. "Thrombotic complications associated with early and late nonadherence to dual antiplatelet therapy." *JACC Cardiovasc Interv* 8 (3):404-10. doi: 10.1016/j.jcin.2014.10.017.

Fujimoto, Y., Y. Kobayashi, and M. Yamaguchi. 2012. "Delamination of Abluminal Polymer of Biolimus-Eluting Stent." *Jacc-Cardiovascular Interventions* 5 (3):E5-E6. doi: 10.1016/j.jcin.2011.09.028.

Hopkins, C. G., P. E. McHugh, and J. P. McGarry. 2010. "Computational Investigation of the Delamination of Polymer Coatings During Stent Deployment." *Annals of Biomedical Engineering* 38 (7):2263-2273. doi: 10.1007/s10439-010-9972-y.

Iakoubovskii, K., K. Mitsuishi, Y. Nakayama, and K. Furuya. 2008. "Mean free path of inelastic electron scattering in elemental solids and oxides using transmission electron microscopy: Atomic number dependent oscillatory behavior." *Physical Review B* 77 (10). doi: ARTN 104102

10.1103/PhysRevB.77.104102.

Jeewandara, T. M., S. G. Wise, and M. K. C. Ng. 2014. "Biocompatibility of Coronary Stents." *Materials* 7 (2):769-786. doi: 10.3390/ma7020769.

Kollum, M., A. Farb, R. Schreiber, K. Terfera, A. Arab, A. Geist, J. Haberstroh, S. Wnendt, R. Virmani, and C. Hehrlein. 2005. "Particle debris from a nanoporous stent coating obscures potential antiproliferative effects of tacrolimus-eluting stents in a porcine model of restenosis." *Catheterization and Cardiovascular Interventions* 64 (1):85-90. doi: 10.1002/ccd.20213.

Kondyurin, Alexey V., Pourandokht Naseri, Jennifer M. R. Tilley, Neil J. Nosworthy, Marcela M. M. Bilek, and David R. McKenzie. 2012. "Mechanisms for Covalent Immobilization of Horseradish Peroxidase on Ion-Beam-Treated Polyethylene." *Scientifica* 2012:28. doi: 10.6064/2012/126170.

Lagerqvist, B., S. K. James, U. Stenestrand, J. Lindback, T. Nilsson, L. Wallentin, and SCAAR Study Grp. 2007. "Long-term outcomes with drug-eluting stents versus bare-metal stents in Sweden." *New England Journal of Medicine* 356 (10):1009-1019. doi: 10.1056/NEJMoa067722.

Oliver, W.C., and G.M. Pharr. 2004. "Measurement of hardness and elastic modulus by instrumented indentation: Advances in understanding and refinements to methodology." *Journal of Materials Research* 19 (01):3-20. doi: doi:10.1557/jmr.2004.19.1.3.

Ormiston, John. 2005. "Polymer Intergrity After CYPHER and TAXUS Stent Implantation: A Scanning Electron Microscopy Study." DES Symposium at TCT 2004.

Otsuka, Y., N. A. Chronos, R. P. Apkarian, and K. A. Robinson. 2007. "Scanning electron microscopic analysis of defects in polymer coatings of three commercially available stents: comparison of BiodivYsio, Taxus and Cypher stents." *J Invasive Cardiol* 19 (2):71-6.

Poncin P, Millet C, Chevy J, Proft JL. 2004. "Comparing and Optimizing Co-Cr Tubing for Stent Applications." Proceedings from the Materials and Processes for Medical Devices Conference.

Seeger, J. M., M. D. Ingegno, E. Bigatan, N. Klingman, D. Amery, C. Widenhouse, and E. P. Goldberg. 1995. "Hydrophilic Surface Modification of Metallic Endoluminal Stents." *Journal of Vascular Surgery* 22 (3):327-336. doi: Doi 10.1016/S0741-5214(95)70148-6.

Slottow, T. L. P., and R. Waksman. 2007. "Overview of the 2006 Food and Drug Administration circulatory system devices panel meeting on drug-eluting stent thrombosis." *Catheterization and Cardiovascular Interventions* 69 (7):1064-1074. doi: 10.1002/ccd.21179.

Vascular, Abbott. 2012. "MULTI-LINK 8 SV, MULTI-LINK 8, and MULTI-LINK 8 LL Coronary Stent System." http://www.abbottvascular.com/docs/ifu/coronary_intervention/eIFU_ML8.pdf.

Waterhouse, A., S. G. Wise, Y. B. Yin, B. C. Wu, B. James, H. Zreiqat, D. R. McKenzie, S. S. Bao, A. S. Weiss, M. K. C. Ng, and M. M. M. Bilek. 2012. "In vivo biocompatibility of a plasma-activated, coronary stent coating." *Biomaterials* 33 (32):7984-7992. doi: 10.1016/j.biomaterials.2012.07.059.

Waterhouse, A., Y. B. Yin, S. G. Wise, D. V. Bax, D. R. McKenzie, M. M. M. Bilek, A. S. Weiss, and M. K. C. Ng. 2010. "The immobilization of recombinant human tropoelastin on metals using a plasma-activated coating to improve the biocompatibility of coronary stents." *Biomaterials* 31 (32):8332-8340. doi: 10.1016/j.biomaterials.2010.07.062.

Yin, Y. B., K. Fisher, N. J. Nosworthy, D. Bax, S. Rubanov, B. Gong, A. S. Weiss, D. R. McKenzie, and M. M. M. Bilek. 2009. "Covalently Bound Biomimetic Layers on Plasma Polymers with Graded Metallic Interfaces for in vivo Implants." *Plasma Processes and Polymers* 6 (10):658-666. doi: 10.1002/ppap.200900045.

Youssef, A. A., H. Hussein, S. K. Hsueh, C. J. Chen, C. H. Yang, C. L. Hang, Y. K. Hsieh, C. Y. Fang, H. K. Yip, and C. J. Wu. 2010. "Cobalt Chromium Coronary Stents and Drug-Eluting Stents in Real Practice." *International Heart Journal* 51 (4):231-237.

APPENDIX

Matlab Code 1 used to calculate the surface stiffness based on unloading displacement vs load for 21 indents from nanoindentation data.

Indentation_code.m

```
n=1;
x=1;
for n=1:1:10
   C=zeros(11,2);
   for x=1:1:11
      C(x,1)=B((P(n,1)+x-1),1);
      C(x,2)=A ((P(n,1)+x-1),1);

       end
   fit=polyfit(C(:,1),C(:,2),1);
   S(n,2)=fit(1,1);
end

figure(1)
loglog(S(:,1),S(:,2),'K.')
```